

# Biomimetic Oxidative Bromination by *cis*-Dioxidotungsten (VI) Complexes of salan type N,N'-Capped Linear Tetradentate Amino Bisphenol

Mannar R. Maurya,<sup>\*,[a]</sup> Shailendra K. Maurya,<sup>[a]</sup> Naveen Kumar,<sup>[a]</sup> and Puneet Gupta<sup>[a]</sup>

Reaction of  $[W^VI O_2(acac)_2]$  (Hacac=acetylacetone) with salan-type dibasic tetradentate ONNO donor Mannich bases derived from ethylenediamine, formaldehyde and 2,4-di-*tert*-butylphenol ( $H_2L^1$ ), 2-*tert*-butyl-4-methylphenol ( $H_2L^2$ ), 2,4-dimethylphenol ( $H_2L^3$ ) and 2,4-dichlorophenol ( $H_2L^4$ ) in a 1:1 ( $[W^VI O_2(acac)_2]:H_2L$ ) molar ratio in refluxing MeOH gave the corresponding *cis*-dioxidotungsten(VI) complexes  $[W^VI O_2L^1]$  (1),  $[W^VI O_2L^2]$  (2),  $[W^VI O_2L^3]$  (3) and  $[W^VI O_2L^4]$  (4), respectively. Characterization by elemental analysis, various spectroscopic (FT-IR, UV-vis,  $^1H$  and  $^{13}C$  NMR) studies, DFT calculations and single-crystal X-ray analysis of 2 and 3 suggest six-coordinated octahedral  $\alpha$ -*cis* (symmetric) isomeric form of the complexes where ligands coordinate through the two phenolate oxygen

and two amine nitrogen atoms (in a *cis*- $\alpha$  type symmetric binding mode) with one of the N atoms of the ligand and one of the terminal O atoms of the *cis*- $WO_2$  group in the axial position. These complexes are potential catalyst precursors for the oxidative bromination of thymol and styrene. Thymol upon bromination gave three products, namely, 2-bromothymol, 4-bromothymol, and 2,4-dibromothymol; later one being the major product. Oxidative bromination of styrene resulted in 2-bromo-1-phenylethanol and 1-phenylethane-1,2-diol; the later one is the result of nucleophilic attack of water on the  $\alpha$  as well as  $\beta$  carbons both of the initially formed 1,2-dibromo-1-phenylethane.

## Introduction

Amongst the third row transition series, tungsten is the only bio-metal known for two families of tungsten containing enzymes: (i) aldehyde oxidoreductases (AORs) and (ii) the formate dehydrogenases (FDHs).<sup>[1,2]</sup> The presence of  $WO_2$  has been proposed in the oxidised active sites of tungstoenzymes, and several model complexes have been prepared to understand their redox chemistry.<sup>[3]</sup> Leaving the chemistry associated with these enzymes, tungsten(VI) complexes having *cis*- $[WO_2]$  moiety have mostly been explored for the catalytic epoxidation of alkenes.<sup>[4–10]</sup> In spite of the good catalytic potentials of these complexes, the growth of the tungsten chemistry, particularly having *cis*- $[WO_2]$  moiety is limited.<sup>[4–13]</sup> After the first report on dioxidotungsten(VI) complexes of hydrogenated analogue of  $H_2salen$  [ $N,N'$ -ethylenebis(salicylideneimine)] (i.e.  $H_2salan$ ) and related ligands,<sup>[13a]</sup> groups of Lehtonen and Mösch-Zanetti have reported dioxidotungsten(VI) complexes of N-methyl derivatives of  $H_2salan$  type ligands.<sup>[9,13b,c]</sup>

Upon metal complex formation  $H_2salan$ , being more flexible than  $H_2salen$  and having better N-basicity, may lead to different

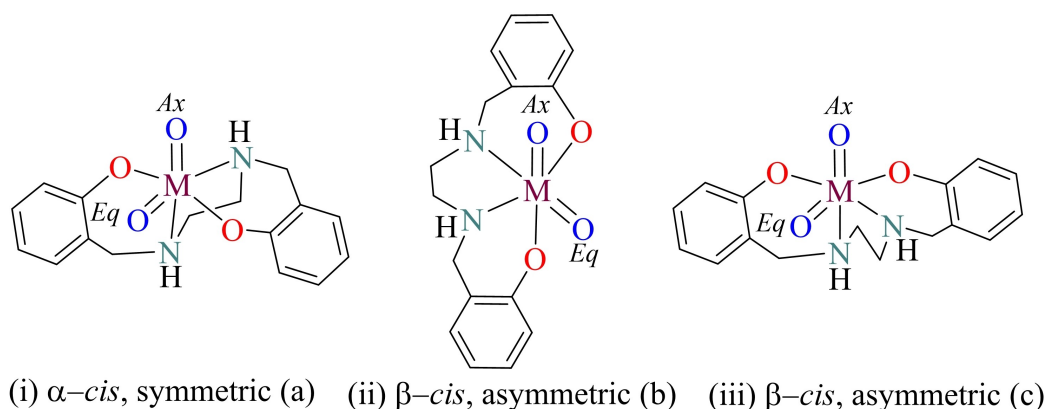
structural conformation which may affect on the catalytic activity of different substrates and selectivity of the product (s).<sup>[14–16]</sup> Considering the location of oxygen atoms (*Ax*, *Eq*) of *cis*- $[MO_2]$  ( $M=V, Mo$  and  $W$ ) complexes, and positions of O and N atoms of such flexible tetradentate ligands in octahedral environment, three different isomeric structures are possible: (i)  $\alpha$ -*cis*, symmetric (a), (ii)  $\beta$ -*cis*, asymmetric (b), and (iii)  $\beta$ -*cis*, asymmetric (c) (Scheme 1).

In *cis*- $[M^VI O_2]$  complexes ( $M=Mo$ <sup>[14,16,18]</sup> or  $W$ <sup>[9]</sup>) of *salen*- and *salan*-type ligands only isomer of the type (a) (i.e.  $\alpha$ -*cis*, symmetric) has been observed whereas isomers (a) and (b) in *cis*- $[VO_2(EDTA)]^{3-}$  ( $H_4EDTA$ =ethylenediamine tetraacetic acid)<sup>[19]</sup> and *cis*- $[VO_2(EDDA)]^-$  ( $H_2EDDA$ =ethylenediamine-N,N'-diacetic acid),<sup>[20]</sup> respectively, have been confirmed by single crystal X-ray study. Based on various spectroscopic studies Crans *et al.* have concluded the presence of species (a) and (b) in equilibrium in a solution of *cis*- $[VO_2(EDDA)]^-$ . They have also argued that the presence of bulky group in case of *cis*- $[VO_2(EDTA)]^-$  is possibly responsible for the isolation of type (a) isomer.

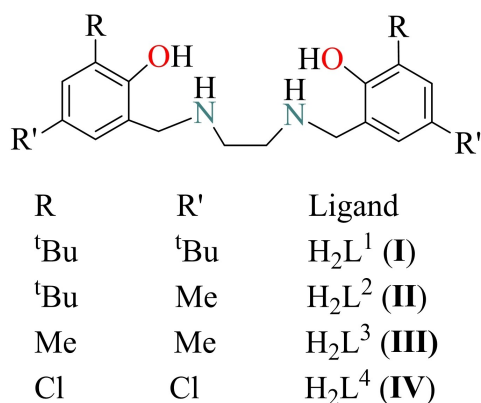
We have prepared herein *cis*- $[W^VI O_2]$  complexes of different derivatives of  $H_2salan$  type N,N'-capped linear tetradentate amino bisphenolate (Scheme 2) with the aims: (i) whether such complexes will adopt the same  $\alpha$ -*cis*, symmetric (a) isomeric structure with more flexible ligands than N-methyl derivatives and if they do adopt the same isomeric structure then why? and (ii) explore them as bioinspired functional model of vanadium haloperoxidase enzymes (V-HPOs). Oxidative halogenation is one of the key reactions shown by V-HPOs.<sup>[21–23]</sup> Such reaction has been of industrial importance as this green procedure deals with the introduction of bromo group(s) into

[a] Prof. Dr. M. R. Maurya, S. K. Maurya, N. Kumar, Dr. P. Gupta  
Department of Chemistry,  
Indian Institute of Technology Roorkee,  
Roorkee-247667, India  
E-mail: m.maurya@cy.iitr.ernet.in  
puneet.gupta@cy.iitr.ac.in  
https://cy.iitr.ac.in/~CY/rkmanfey  
https://cy.iitr.ac.in/~CY/Puneet\_Gupta

Supporting information for this article is available on the WWW under  
https://doi.org/10.1002/ejic.202100357



**Scheme 1.** Three different possible isomeric structures for octahedral complexes having *cis*-[MO<sub>2</sub>] (M = V, Mo and W) moiety: (i)  $\alpha$ -cis, symmetric (a), (ii)  $\beta$ -cis, asymmetric (b) and (iii)  $\beta$ -cis, asymmetric (c).  $\alpha$ -Cis, symmetric represents two terminal Os of *cis*-MO<sub>2</sub> in *trans* position to both Ns, and  $\beta$ -cis, asymmetric represents one terminal O of *cis*-MO<sub>2</sub> *trans* to N and other one *trans* to O. Nomenclatures are partly adopted from references 16 and 17. All structures are drawn considering Z-axis as the axial sites.



**Scheme 2.** Structure of ligands and their abbreviations used in this study.

organic molecules. While *cis*-[V<sup>VI</sup>O<sub>2</sub>] complexes<sup>[24–29]</sup> (and *cis*-[M<sup>VI</sup>O<sub>2</sub>] complexes<sup>[30,31]</sup> to a less extent) have been used as functional mimics (oxidative bromination in particular) of V-HPO enzymes, except one report from our group, *cis*-[W<sup>VI</sup>O<sub>2</sub>] complexes have not been explored for the oxidative bromination of organic substrates.

## Results and Discussion

Ligands H<sub>2</sub>L<sup>1–4</sup> (I–IV) are similar to H<sub>2</sub>salan-type ligands<sup>[9,14]</sup> but are obtainable through a rather simple Mannich condensation between ethylenediamine, formaldehyde and 2,4-disubstituted phenols<sup>[18]</sup> in good yields. These ligands react with [W<sup>VI</sup>O<sub>2</sub>(acac)<sub>2</sub>] in 1:1 molar ratio in refluxing MeOH to yield corresponding dioxidotungsten(VI) complexes, [W<sup>VI</sup>O<sub>2</sub>L<sup>1</sup>] (1), [W<sup>VI</sup>O<sub>2</sub>L<sup>2</sup>] (2), [W<sup>VI</sup>O<sub>2</sub>L<sup>3</sup>] (3) and [W<sup>VI</sup>O<sub>2</sub>L<sup>4</sup>] (4), respectively. These complexes are cream coloured and soluble in MeOH, EtOH, CHCl<sub>3</sub>, MeCN, DMF and DMSO. Elemental analyses and various spectroscopic (FT-IR, UV-vis, <sup>1</sup>H and <sup>13</sup>C NMR) studies confirm the formation of complexes. However, single-crystal X-ray analysis of complexes

2 and 3 confirms the isolation of  $\alpha$ -cis, symmetric (a) (c.f. Scheme 1) isomer only in the solid state.

## Thermal Study

All complexes are thermally stable up to 280 °C and there after decompose in two major steps. First step starts at ca. 280 °C and completes with 8–30% mass loss at ca. 306 °C. Second step starts immediately after first step and completes at ca. 500 °C with the formation of WO<sub>3</sub>. The observed WO<sub>3</sub> content of 33.0% for 1, 36.0% for 2, 42.0% for 3, and 37.0% for 4 match well with the calculated value of 32.6% for 1, 37.0% for 2, 42.4% for 3 and 37.2% for 4 (Figure S1), respectively.

## Structure Descriptions of Complexes 2 and 3

The coordination functionality of ligands and the resulting geometry around the tungsten centre was confirmed by SC-XRD studies. ORTEPs for the compounds [W<sup>VI</sup>O<sub>2</sub>L<sup>2</sup>] (2) and [W<sup>VI</sup>O<sub>2</sub>L<sup>3</sup>] (3) are presented in Figure 1 and Figure 2, respectively. Selected bond distances and angles are given in Table 1.

The structure of six-coordinated complexes 2 and 3 adopt a distorted octahedral geometry with two O<sub>oxido</sub> terminal oxygen atoms, two O<sub>phenolate</sub> and two N<sub>amine</sub> atoms of ligands. The axial sites are occupied by the terminal O<sub>oxido</sub> atom [O(1)] and the nitrogen atoms [N(1)] of the ligand while the other terminal O<sub>oxido</sub> [O(2)], two O<sub>phenolate</sub> [O(3) and O(4)], and one N<sub>amine</sub> [N(2)] atoms of ligands are arranged in equatorial position<sup>[9,14,17–19]</sup>. Thus, the structure belongs to  $\alpha$ -cis, symmetric (a) (c.f. Scheme 1) type isomer, a common isomeric form found in most complexes having *cis*-[MO<sub>2</sub>] (M = V, Mo and W) structure and two nitrogen atoms are in a *cis*- $\alpha$  type binding mode.<sup>[9,14,17–19]</sup> The equatorial plane is distorted with respect to the planarity. The tungsten atom is displaced toward the apical oxido ligand, O(1), from the equatorial plane defined by N(2), O(2), O(3) and

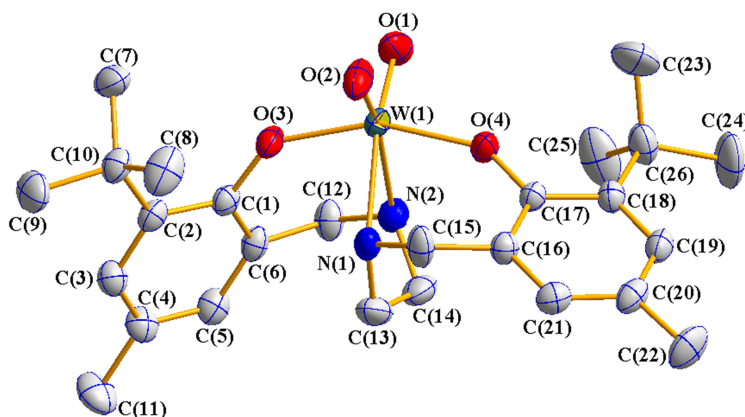


Figure 1. ORTEP of  $[W^VI O_2 L^2]$  (2). All the non-hydrogen atoms are presented by their 50% probability ellipsoids. Hydrogen atoms are omitted for clarity.

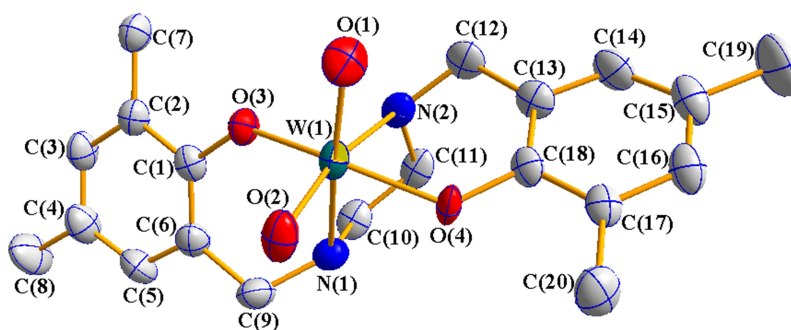


Figure 2. ORTEP of  $[W^VI O_2 L^3]$  (3). All the non-hydrogen atoms are presented by their 50% probability ellipsoids. Hydrogen atoms are omitted for clarity.

Table 1. Bond lengths [Å] and angles [°] for  $[W^VI O_2 L^2]$  (2) and  $[W^VI O_2 L^3]$  (3).

Bond	2	3
W(1)–O(1)	1.724(2)	1.720(4)
W(1)–O(2)	1.721(2)	1.727(3)
W(1)–O(3)	1.950(2)	1.949(2)
W(1)–O(4)	1.9248(19)	1.947(3)
W(1)–N(1)	2.334(2)	2.347(3)
W(1)–N(2)	2.354(3)	2.314(3)
Angle	2	3
O(1)–W(1)–O(2)	106.19(12)	107.66(14)
O(1)–W(1)–O(4)	93.74(9)	99.00(17)
O(2)–W(1)–O(4)	99.82(9)	96.39(11)
O(1)–W(1)–O(3)	98.93(10)	96.52(14)
O(2)–W(1)–O(3)	95.40(9)	98.80(12)
O(4)–W(1)–O(3)	156.64(8)	153.85(12)
O(1)–W(1)–N(1)	163.65(11)	164.78(13)
O(2)–W(1)–N(1)	89.73(11)	87.19(13)
O(4)–W(1)–N(1)	79.58(8)	82.18(12)
O(3)–W(1)–N(1)	82.89(8)	77.45(10)
O(1)–W(1)–N(2)	91.09(11)	91.84(13)
O(2)–W(1)–N(2)	162.65(11)	160.39(12)
O(4)–W(1)–N(2)	80.14(9)	78.06(10)
O(3)–W(1)–N(2)	80.08(8)	80.53(11)
N(1)–W(1)–N(2)	73.14(9)	73.48(11)

O(4), by 0.009 Å in 2 and 0.010 Å in 3. The W–O<sub>oxido</sub> bond lengths [W(1)–O(1): 1.724(2) in 2 and 1.720(4) in 3, and W(1)–O(2): 1.721(2) in 2 and 1.727(3) in 3] and O=W=O bond

angle [106.19(12)° in 2, and 107.66(14)° in 3] (see Table 1) are well within the range for the bond distances and angles typically observed in these types of compounds.<sup>[9,14,17,18]</sup> Inter-molecular hydrogen bonds were observed in compounds 2 and 3 (see Table 2). The crystal packing (see Figure S2 and Figure S3) of the complexes 2 and 3 confirms that they have 8 and 4 molecules per unit cell, respectively.

### IR Spectral Study

The IR spectral analysis of the ligands and complexes was carried out to ascertain the coordination modes of the ligands in complexes. Selected IR bands are presented in the experimental section. The presence of two characteristics IR bands at 886–901 and 922–942 cm<sup>−1</sup> due to the  $\nu_{\text{sym}}(\text{O}=\text{W}=\text{O})$  and  $\nu_{\text{asym}}(\text{O}=\text{W}=\text{O})$  stretches, respectively, approves the *cis*-[WO<sub>2</sub>] core in these complexes.<sup>[7,9,11,13]</sup> All ligands display a broad band around 3200 cm<sup>−1</sup> due to  $\nu(\text{OH})$  of the phenol and absence of this band in complexes suggests the coordination of phenolate O after deprotonation. Ligands as well as complexes both exhibit a broad band at 3050–3300 cm<sup>−1</sup> due to  $\nu(\text{NH})$  stretch, hence, the coordination of N could not be established explicitly. However, the coordination of N, at least, in two complexes and N as well as O in all complexes are well supported by the SC-XRD and NMR studies, respectively.

**Table 2.** Hydrogen bonds for [W<sup>VI</sup>O<sub>2</sub>L<sup>2-</sup>] (2) and [W<sup>VI</sup>O<sub>2</sub>L<sup>3-</sup>] (3).<sup>[a]</sup>

Compound	D—H...A	d(D—H)	d(H...A)	d(D...A)	∠(DHA)
2	C(15)—H(15B)...O(1)#2	0.970(1)	2.226(1)	2.997(2)	135.61(4)
3	N(2)—H(2 N)...O(2)#1	0.98(1)	1.907(2)	2.840(3)	158.28(1)

[a] Symmetry transformations used to generate equivalent atoms: #1  $-x+3/2, y+1/2, -z+3/2$  #2  $x+1/2, y, -z+3/2$ .

## UV-visible Spectral Study

UV-vis spectral data of ligands and their *cis*-[W<sup>VI</sup>O<sub>2</sub>] complexes recorded in MeCN (for spectra see Figure S4). The UV-vis spectra of the ligands display two spectral bands at 224–236 and 282–292 nm<sup>[18]</sup> which are assigned to  $\pi \rightarrow \pi^*$  and  $n \rightarrow \pi^*$  transitions, respectively. These transitions undergo red and blue shift, respectively, in metal complexes. Coordination of ligands' functionality to the metal ion thereby restructuring of ligands possibly causing such changes. Surprisingly, we did not observe ligand to metal charge transfer transition in all complexes even in any solvent at any concentration. The possible reason for this could be that they are either too high or too low in energy and fall outside the visible part of the spectrum.

## <sup>1</sup>H NMR Spectral Study

<sup>1</sup>H NMR spectra of ligands and complexes recorded in d<sub>6</sub>-[DMSO] are presented in Table 3; spectra of H<sub>2</sub>L<sup>2-</sup> (II) and the corresponding complex 2 as representative of the series are reproduced in Figure 3. The disappearance a signal in complexes, which appears at  $\delta = 10.21$ – $10.93$  ppm in ligands due to two phenolic —OH protons, suggests the coordination of the phenolic oxygen to the metal after their deprotonation. The —NH protons resonate as a sharp band at  $\delta = 3.28$ – $3.39$  ppm in I, II and III and as a relatively broad signal at  $\delta = 5.12$  ppm in IV. Possibly due to redistribution of electron density upon coordination of nitrogen to the metal, this signal slightly shifts in the corresponding complexes. The isomer  $\alpha$ -*cis* (a) (*c.f.* Scheme 1) proposed for all complexes and confirmed for 2 and 3 by single crystal X-ray diffraction study is non-planar while ligands are

symmetrical in nature. These make the protons of two individual ArCH<sub>2</sub>N— groups as well as the —CH<sub>2</sub>CH<sub>2</sub>— protons non-equivalent. Accordingly, ArCH<sub>2</sub>N— protons appear as two doublets [e.g. at 4.70 (d, 2H) and 3.90 (d, 2H) ppm for 1] while ligands exhibit only one singlet at  $\delta = 3.78$ – $3.91$  ppm. Similarly, the —CH<sub>2</sub>CH<sub>2</sub>— protons appearing as singlet at  $\delta = 2.70$ – $2.94$  ppm in ligands split into two triplets (Table 3). Such observations have also been noted in similar dioxidotungsten (VI)<sup>[9]</sup> as well as dioxidomolybdenum(VI) complexes.<sup>[9,14, 18]</sup>

## <sup>13</sup>C NMR Spectral Study

<sup>13</sup>C NMR spectral data recorded in d<sub>6</sub>-[DMSO] are accessible in Table 4; complex 3 along with the corresponding ligand as representative of the series are reproduced in Figure 4. The coordination-induced chemical shift [ $\Delta\delta = \delta(\text{complex}) - \delta(\text{ligand})$ ], extracted from <sup>13</sup>C NMR spectral data further supports the binding modes of the ligands to the metal centre. Thus, the carbons C1/C1' bearing the phenolic oxygen of ligands undergo a shift,  $\Delta\delta$  between 1.68 to  $-0.9$  ppm (see Table 4) after coordination with tungsten centre. Similarly, the effect of coordination of nitrogen on the ethylenic carbons (C8/C8') as well as benzylic carbons (C7/C7') is also significant as they resonate with an average shift of  $\Delta\delta$  between 0.16 to  $-4.96$  ppm and 2.06 to  $-4.57$  ppm, respectively. All other carbons resonate well within the expected regions. Existence of more than one species in solution have been observed by Coreia *et al.*<sup>[17]</sup> and Crans *et al.*,<sup>[20]</sup> in *cis*-VO<sub>2</sub> complexes. Since <sup>13</sup>C NMR spectra of complexes exhibit only one signal each for C7/C7' and C8/C8', the presence of only one species in solution under the specified condition is suggested, and splitting of

**Table 3.** <sup>1</sup>H NMR (500 MHz) data ( $\delta$  in ppm) of ligands and their complexes in d<sub>6</sub>-[DMSO].

Compounds	—OH	—NH	Aryl (J in Hz)	ArCH <sub>2</sub> N—	—CH <sub>2</sub> CH <sub>2</sub> —	CH <sub>3</sub>
H <sub>2</sub> L <sup>1</sup> (I)	10.93 (s, 2H)	3.38 (s, 2H)	7.09 (d, 2H, J = 2), 6.86 (d, 2H, J = 1.5)	3.87 (s, 4H)	2.93 (s, 4H)	1.35 (s, 18H), 1.21 (s, 18H)
[W <sup>VI</sup> O <sub>2</sub> L <sup>1-</sup> ] (1)	—	4.62 (s, 2H)	7.18 (d, 2H, J = 2), 6.96 (d, 2H, J = 2)	4.70 (d, 2H), 3.90 (d, 2H)	2.94 (t, 2H), 2.36 (t, 2H)	1.37 (s, 18H), 1.25 (s, 18H)
H <sub>2</sub> L <sup>2</sup> (II)	10.76 (s, 2H)	3.28 (s, 2H)	6.86 (d, 2H, J = 1.5), 6.65 (d, 2H, J = 1.5)	3.82 (s, 4H)	2.94 (s, 4H)	2.13 (s, 6H), 1.33 (s, 18H)
[W <sup>VI</sup> O <sub>2</sub> L <sup>2-</sup> ] (2)	—	4.58 (s, 2H)	6.97 (d, 2H, J = 1.5), 6.77 (d, 2H, J = 1.5)	4.69 (d, 2H), 3.82 (d, 2H)	2.93 (t, 2H), 2.35 (t, 2H)	2.21 (s, 6H), 1.35 (s, 18H)
H <sub>2</sub> L <sup>3</sup> (III)	10.21 (s, 2H)	3.39 (s, 2H)	6.79 (d, 2H, J = 1.5), 6.68 (d, 2H, J = 1.5)	3.78 (s, 4H)	2.85 (s, 4H)	2.13 (s, 6H), 2.09 (s, 6H)
[W <sup>VI</sup> O <sub>2</sub> L <sup>3-</sup> ] (3)	—	5.12 (s, 2H)	6.89 (d, 2H, J = 2), 6.73 (d, 2H, J = 2)	4.73 (d, 2H), 3.81 (d, 2H)	2.83 (t, 2H), 2.32 (t, 2H)	2.18 (s, 6H), 2.14 (s, 6H)
H <sub>2</sub> L <sup>4</sup> (IV)	—	—	7.33 (d, 2H, J = 2), 7.12 (d, 2H, J = 2)	3.91 (s, 4H)	2.70 (s, 2H)	—
[W <sup>VI</sup> O <sub>2</sub> L <sup>4-</sup> ] (4)	—	5.61 (s, 2H)	7.50 (d, 2H, J = 2.5), 7.26 (d, 2H, J = 2.5)	4.73 (d, 2H), 3.99 (d, 2H)	2.94 (t, 2H), 2.26 (t, 2H)	—

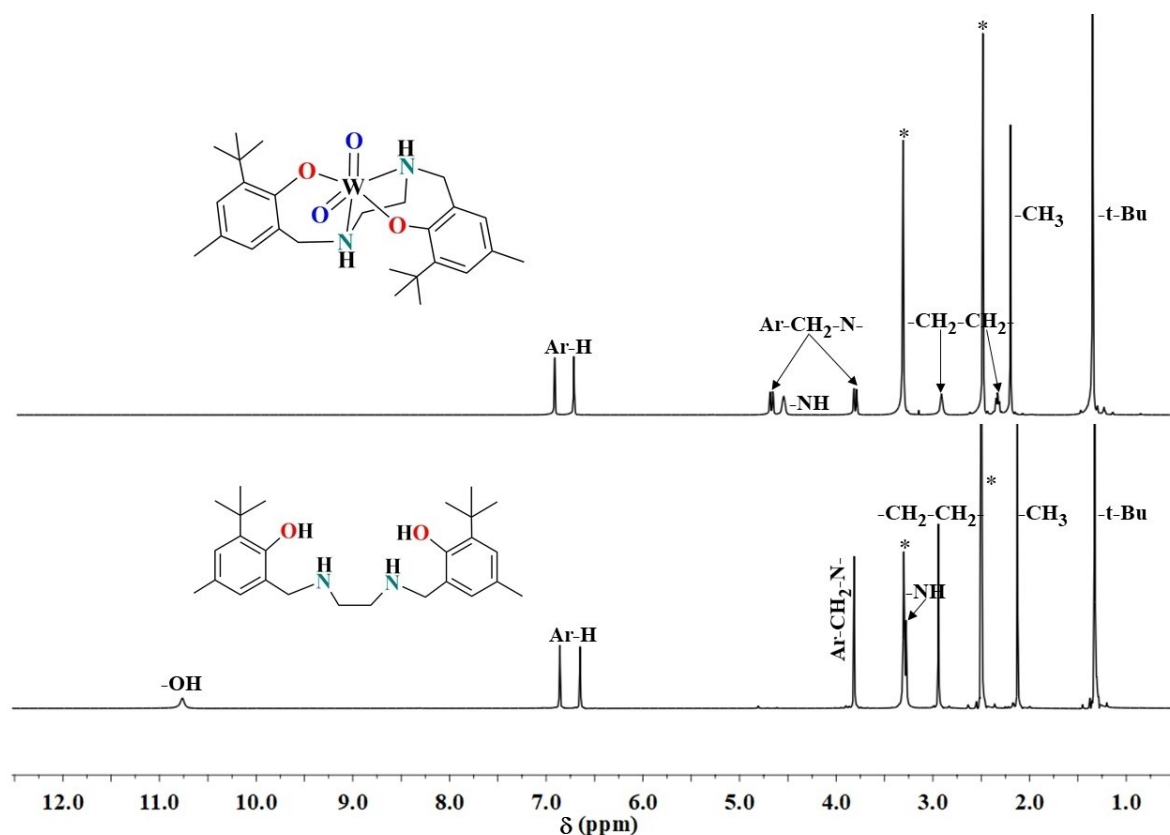
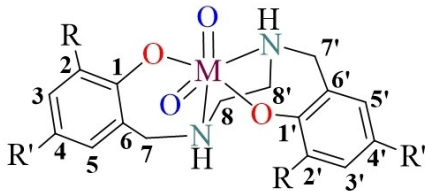


Figure 3.  $^1\text{H}$  NMR spectra of  $\text{H}_2\text{L}^2$  (II) and  $[\text{W}^{\text{VI}}\text{O}_2\text{L}^2]$  (2). \* indicates signals due to water or DMSO.

Table 4.  $^{13}\text{C}$  NMR spectral data of ligands and complexes recorded in  $\text{d}_6$ -[DMSO].

					
R = R' = t-but, Me, Cl (for detail see Scheme 2)					
Compounds	C1/C1'	C7/C7'	C8/C8'	R/R'	Other Carbons
$\text{H}_2\text{L}^1$ (I)	153.65	57.85	50.95	31.44, 29.43	139.8, 134.5, 122.9, 122.1, 121.3, 34.4, 33.7
$[\text{W}^{\text{VI}}\text{O}_2\text{L}^1]$ (1)	155.12 (1.47)	53.28 (−4.57)	46.50 (−4.45)	31.46, 30.98	141.3, 137.6, 123.8, 121.9, 121.5, 34.7, 33.9
$\text{H}_2\text{L}^2$ (II)	153.62	57.32	50.79	29.34, 20.34	135.2, 126.7, 126.3, 126.1, 122.0, 34.1
$[\text{W}^{\text{VI}}\text{O}_2\text{L}^2]$ (2)	155.20 (1.58)	52.94 (−4.38)	46.40 (−4.39)	29.92, 20.40	138.3, 127.9, 127.5, 125.9, 122.0, 34.4
$\text{H}_2\text{L}^3$ (III)	152.70	56.47	50.89	20.00, 15.52	130.1, 126.7, 126.5, 123.5, 121.5
$[\text{W}^{\text{VI}}\text{O}_2\text{L}^3]$ (3)	154.38 (1.68)	52.59 (−3.88)	45.93 (−4.96)	20.01, 16.54	129.7, 128.1, 127.2, 126.9, 121.2
$\text{H}_2\text{L}^4$ (IV)	153.76	50.04	46.27	–	127.3, 127.0, 126.4, 120.9, 120.7
$[\text{W}^{\text{VI}}\text{O}_2\text{L}^4]$ (4)	152.86 (−0.9)	52.10 (2.06)	46.43 (0.16)	–	128.0, 127.7, 125.7, 124.1, 123.5

protons associated with these carbons are only due to non-planarity.

#### Cyclic Voltammetry Study

The voltammograms of complexes 1 and 3 (Figure 5) exhibit only one reductive peak at  $-1.24$  and  $-1.02$  V as well as only one oxidative peak at  $1.44$  and  $1.56$  V, respectively, which are



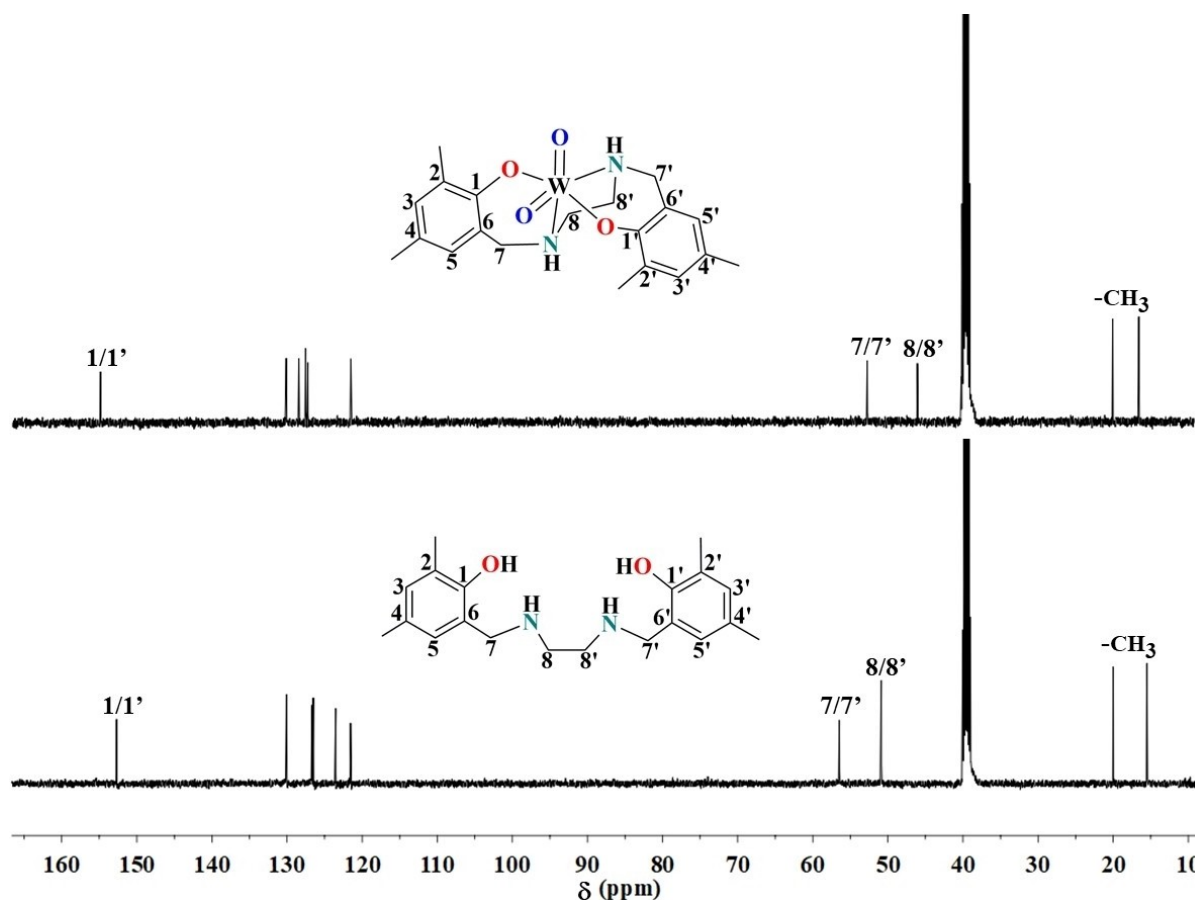


Figure 4.  $^{13}\text{C}$  NMR of spectra of  $\text{H}_2\text{L}^3$  (III) and  $[\text{W}^{\text{VI}}\text{O}_2\text{L}^3]$  (3). Broad multiplex is due to DMSO.

due to  $\text{W(VI)} \rightarrow \text{W(V)}$  redox processes. Reductive peak of complex 1 is reversible in nature, while other peaks of complexes 1 and 3 are irreversible in nature. These peaks are also supported by differential pulse voltammetry (DPV), where complex 1 and 3 shows one reductive peak each at  $-1.14$  and  $-0.88$  V and one oxidative peak each at  $1.38$  and  $1.49$  V, respectively. In complex 2, one reductive peak at  $-1.18$  V due to  $\text{W(VI)} \rightarrow \text{W(V)}$  could be observed but two oxidative peaks at  $1.49$  and  $1.96$  V of irreversible nature are seen which are attributed to  $\text{W(IV)} \rightarrow \text{W(V)}$  and  $\text{W(V)} \rightarrow \text{W(VI)}$  processes (Figure 5). This is further confirmed by their DPV which shows one reductive peak at  $-1.05$  V and two oxidative peaks at  $1.39$  and  $1.80$  V. However, complex 4 shows (Figure 5) two reductive peak at  $-0.68$  and  $-1.36$  V and only one oxidative peak at  $2.03$  V which correspond to the  $\text{W(VI)} \rightarrow \text{W(V)} \rightarrow \text{W(IV)}$  and  $\text{W(V)} \rightarrow \text{W(VI)}$  redox process respectively, and these are irreversible in nature. Their DPV also shows two reductive peaks at  $-0.92$  and  $-1.29$  V and one oxidative peak at  $1.83$  V. While no information on the electrochemical behaviour of similar  $\text{cis-}[\text{W}^{\text{VI}}\text{O}_2]$  complexes is available, the analogous  $[\text{Mo}^{\text{VI}}\text{O}_2(\text{salan})]$  complex with no substituent at phenolic group shows irreversible electrochemical behaviour in DMF but no further details are available. Therefore, results obtained here cannot be compared directly with this complex. However, complexes of N,N'-dimethyl derivative of  $\text{H}_2\text{salan}$

having *p*-substituents on phenyl ring show quasi-reversible electrochemical behaviour.<sup>[14]</sup> The more negative reduction potential, the more difficult for the *cis-}[\text{W}^{\text{VI}}\text{O}\_2] complexes to be reduced. Hence, the reduction of complexes follows the order:  $4 < 1 < 2 < 3$ . The electron withdrawing group leads to the shifting of the reduction potential in these complexes towards less negative value. The observed CV data of all ligands and complexes along with corresponding DPV are given in Table 5.*

### Density Functional Theory Study

DFT calculations were taken up to compute the relative stability of the three possible isomeric forms:  $\alpha$ -*cis*, symmetric (a),  $\beta$ -*cis*, asymmetric (b), and  $\beta$ -*cis*, asymmetric (c) as proposed for *cis-}[\text{WO}\_2] complexes in Scheme 1 and to understand whether optimised structures also suggest same configuration of complexes as have been observed by single crystal X-ray study. DFT calculations were performed employing the ORCA4.2 quantum chemical program package.<sup>[21]</sup> The relative Gibbs free energies reported in our DFT studies were obtained at the BP86<sup>[22,23]</sup>-D3<sup>[24]</sup>/def2-SVP<sup>[25]</sup> level. All Gibbs free energies reported in our studies are in  $\text{kcal.mol}^{-1}$  and relative to the computational model for  $\alpha$ -*cis*, symmetric (a). A relative stability*

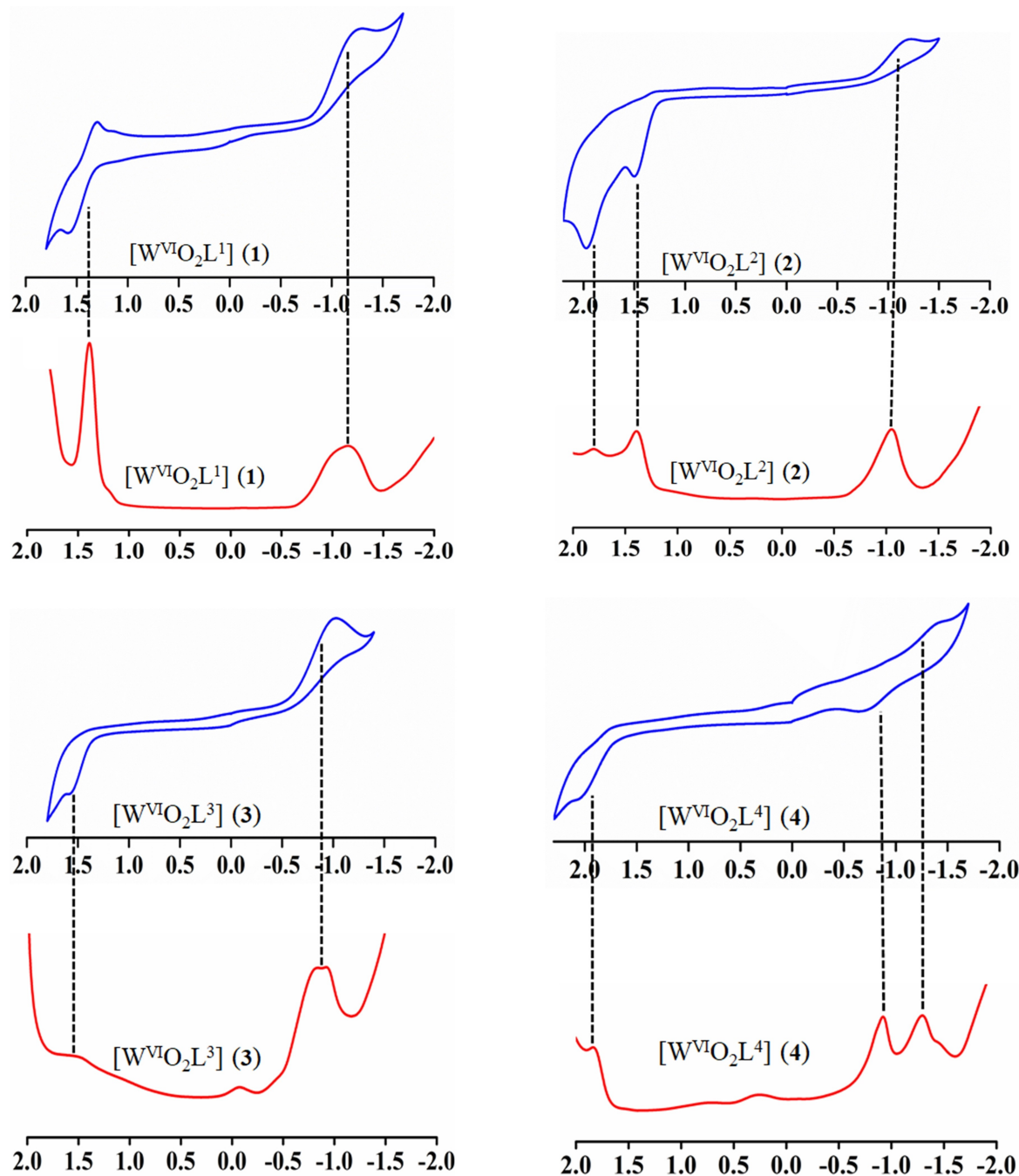


**Figure 5.** CV plot of complexes  $[W^{VI}O_2L^1]$  (1),  $[W^{VI}O_2L^2]$  (2),  $[W^{VI}O_2L^3]$  (3) and  $[W^{VI}O_2L^4]$  (4) along with the corresponding DPV plot. Conditions: room temperature (ca. 298 K) in DMF, [complex] = 1 mM, [TBAPF<sub>6</sub>] = 0.2 M, scan speed 100 mV/s, Pt working electrode, Ag/AgCl reference electrode and Pt wire as counter electrode.

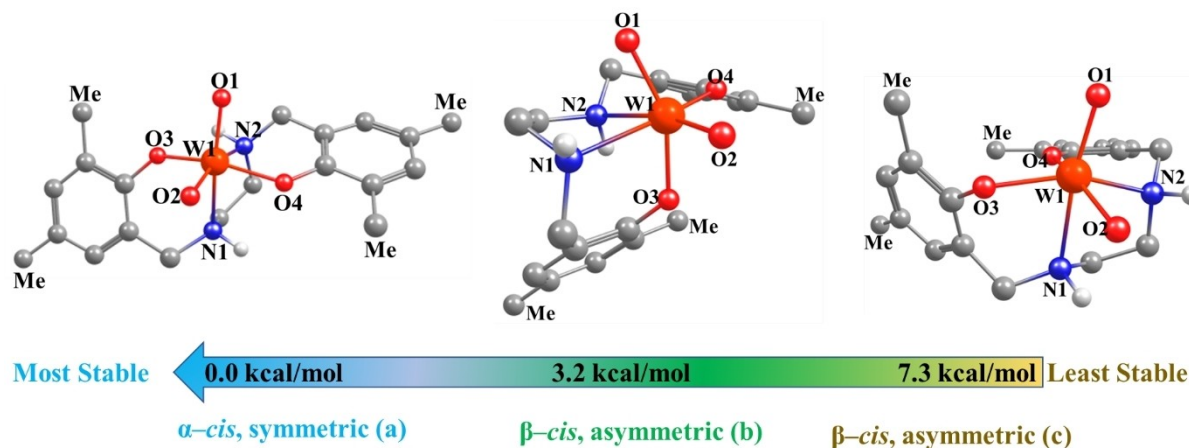
comparison of the three isomers for the ligand  $H_2L^3$  (i.e. methyl substituents at phenol) is presented in Figure 6. The isomer  $\alpha$ -*cis*, symmetric (a) is 3.2 kcal.mol<sup>-1</sup> more stable than the  $\beta$ -*cis*, asymmetric (b), whereas the isomer  $\beta$ -*cis*, asymmetric (c) is found to be 7.3 kcal/mol less stable as compared to the isomer  $\alpha$ -*cis*, symmetric (a), therefore,  $\beta$ -*cis* (c) is not modelled for rest of the ligand types. For the two isomers [ $\alpha$ -*cis*, symmetric (a) and  $\beta$ -*cis*, asymmetric (b)], the *cis*-[WO<sub>2</sub>] complexes of all four ligand systems ( $H_2L^1$ – $H_2L^4$ , Scheme 2) were considered to

construct the computational models. The relative energies results are presented in Table 6. Our computations show that for all four complexes 1–4, the isomer  $\alpha$ -*cis*, symmetric (a) is more stable than the  $\beta$ -*cis*, asymmetric (b). The relative stability results are in agreement with the structures solved by single crystal X-ray study where only  $\alpha$ -*cis*, symmetric (a) isomer was found. This observation is also in line with the argument given by Crans *et al.* that bulky groups present on the ligand system may facilitated to move  $\alpha$ -*cis*, symmetric isomer to  $\beta$ -*cis*,

**Table 5.** Cyclic voltammetric (CV) and differential pulse voltammetric (DPV) results for ligands and dioxidotungsten(VI) complexes at 298 K.

Compounds	Epa[V] <sup>[a]</sup>	Epc[V] <sup>[a]</sup>	DPV
H <sub>2</sub> L <sup>1</sup> (I)	1.43	−1.37	−1.14, 1.53
[W <sup>VI</sup> O <sub>2</sub> L <sup>1</sup> ] (1)	1.44	−1.24	−1.14, 1.38
H <sub>2</sub> L <sup>2</sup> (II)	1.24	−1.43	−1.19, 0.94
[W <sup>VI</sup> O <sub>2</sub> L <sup>2</sup> ] (2)	1.49, 1.96	−1.18	−1.05, 1.39, 1.80
H <sub>2</sub> L <sup>3</sup> (III)	1.06	−0.71	−1.03, 1.04
[W <sup>VI</sup> O <sub>2</sub> L <sup>3</sup> ] (3)	1.56	−1.02	−0.88, 1.49
H <sub>2</sub> L <sup>4</sup> (IV)	1.10	−0.55, −1.14	−0.57, −1.09, 1.18
[W <sup>VI</sup> O <sub>2</sub> L <sup>4</sup> ] (4)	2.03	−0.68, −1.36	−0.92, −1.29, 1.83

[a] Epa and Epc are the anodic and cathodic peak potentials vs SCE, respectively.

**Figure 6.** A relative stability comparison of the three isomers for the ligand H<sub>2</sub>L<sup>1</sup>. Hydrogens attached to carbons are not shown to enhance the clarity.**Table 6.** DFT computed relative Gibbs free energies of the isomers *α-cis* (a) and *β-cis* (b) (see Scheme 1) for *cis*-[WO<sub>2</sub>L] complexes 1–4.

Complex with substituents	Isomer <i>α-cis</i> (a) Gibbs Free Energy (kcal.mol <sup>−1</sup> )	Isomer <i>β-cis</i> (b) Gibbs Free Energy (kcal.mol <sup>−1</sup> )
1: R = R' = 'Bu	0.0	2.8
2: R = 'Bu, R' = Me	0.0	3.6
3: R = R' = Me	0.0	3.2
4: R = R' = Cl	0.0	3.8

asymmetric in solution<sup>[20]</sup> as Gibbs free energies difference is less in case of 'Bu substituents than that having chloro substituents (2.8 vs 3.8 kcal mol<sup>−1</sup>). DFT optimized structures of *α-cis*, symmetric (a) and *β-cis*, asymmetric (b), are presented in Figure 7 and Figure 8. Geometrical parameters obtained from DFT computations for these isomers are summarized in Table S1 and Table S2. These bond lengths and angles are also comparable to the ones obtained through SC-XRD within the acceptable limit.

### Catalytic Activity Studies

**Oxidative Bromination of Thymol** – Vanadium complexes studied as functional models of V-HPOs play an important role not only in brominating the organic molecules but in establishing the possible reaction pathway as well. During the catalytic oxidative bromination by vanadium,<sup>[26–29]</sup> the formation of an

intermediate oxido(peroxido) species has been proposed which allows nucleophilic attack of the bromide ion, followed by release of HOBr/Br<sub>2</sub> which actually brominates the substrates. The *cis*-[WO<sub>2</sub>] complexes, 1–4 reported here act as catalyst precursor to brominate thymol and styrene in the presence of KBr, 30% aqueous H<sub>2</sub>O<sub>2</sub>, and 70% aqueous HClO<sub>4</sub> in aqueous medium. Phenol being *ortho*- and *para*-directing, the bromination on thymol takes place on the most activated site and gives three products, namely, 2-bromothymol, 4-bromothymol, and 2,4-dibromothymol (Scheme 3); further bromination of mono-bromo products possibly gives 2,4-dibromothymol.<sup>[30–34]</sup> These are the usual products reported in the literature.<sup>[30–34]</sup>

As pointed out in the experimental section (vide infra) the reaction conditions were optimised considering 2 as a representative catalyst to obtain the maximum yield of brominated products. Thus, for 10 mmol of thymol (1.50 g), four different amounts of catalyst (0.5, 1.0, 1.5 and 2.0 mg), three different amounts of 30% aqueous H<sub>2</sub>O<sub>2</sub> (10, 15 and 20 mmol) and three



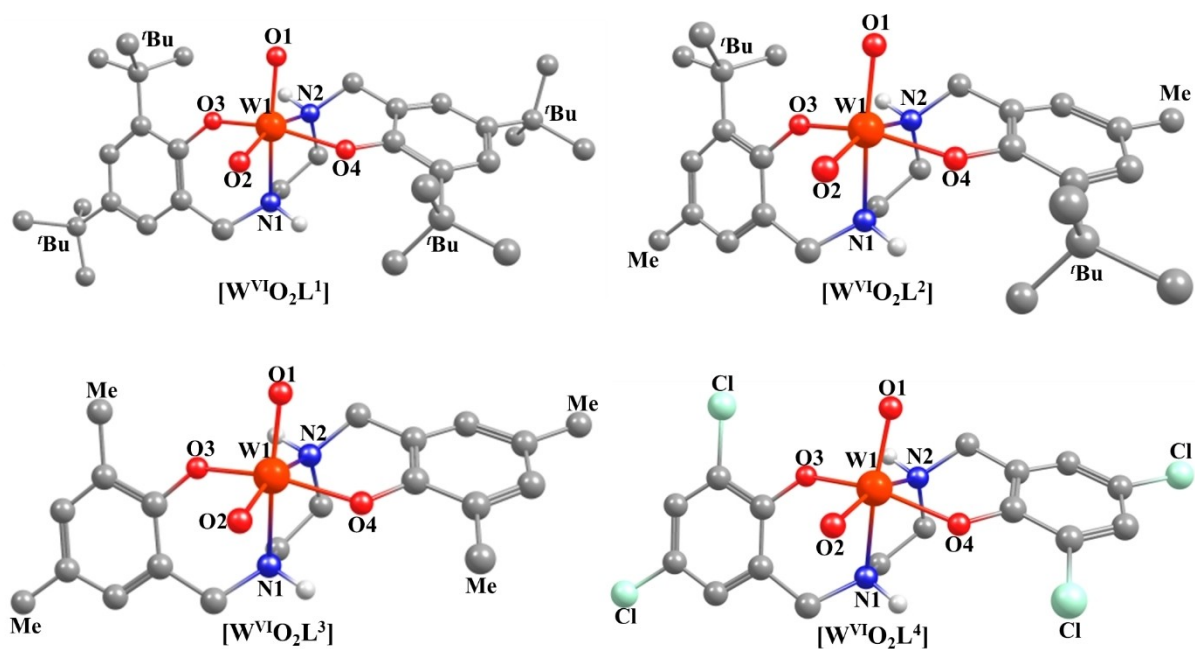


**Figure 7.** DFT computed structures of the isomer  $\alpha$ -cis, symmetric (a) for different  $cis$ -[WO<sub>2</sub>] complexes. Hydrogens attached to carbons are not shown to enhance the clarity.

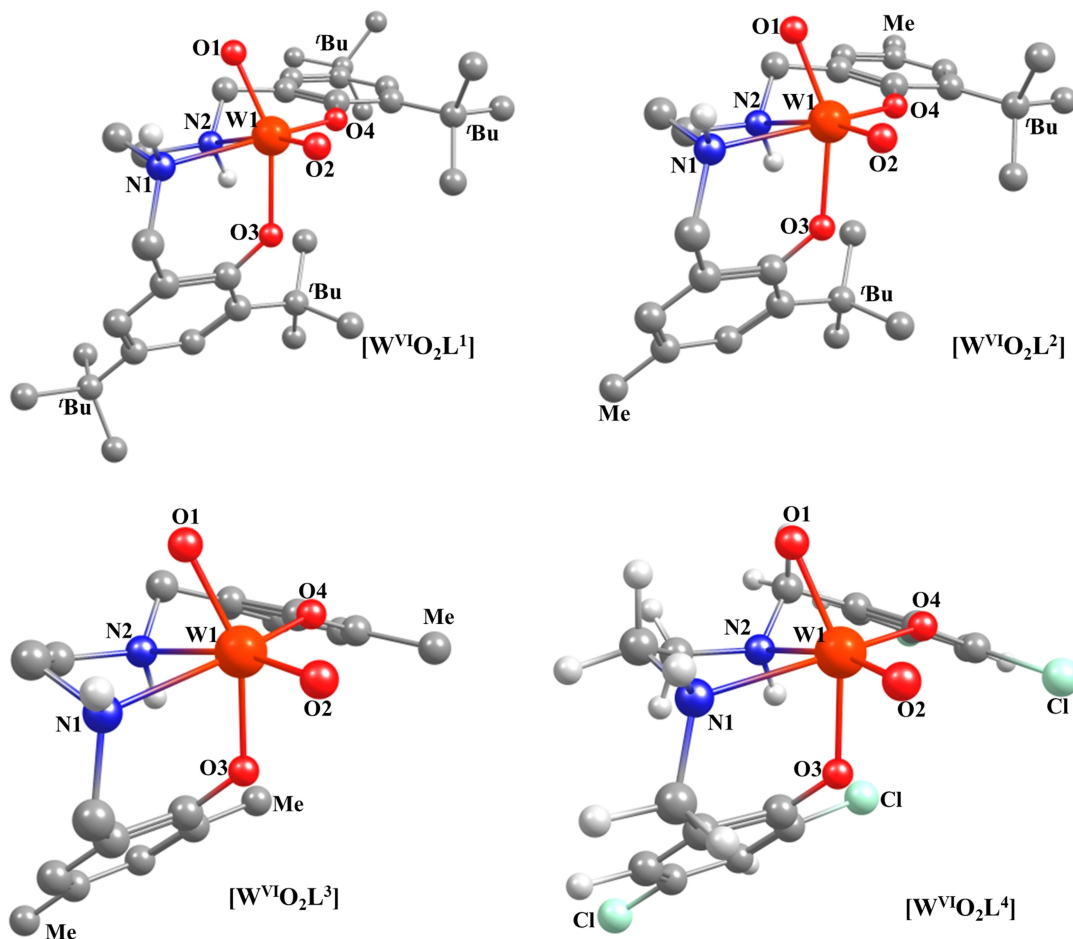
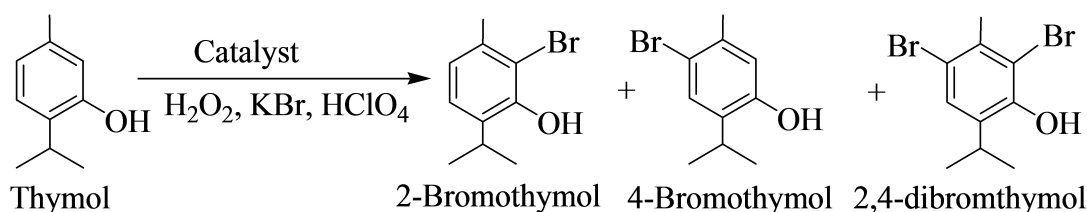


**Figure 8.** DFT computed structures of the isomer  $\beta$ -cis, asymmetric (b) for different  $cis$ -[WO<sub>2</sub>] complexes. Hydrogens attached to carbons are not shown to enhance the clarity.



**Scheme 3.** Products of the oxidative bromination of thymol.

**Table 8.** Conversions, turn over frequency and selectivity parameters for various catalysts for the oxidative bromination of thymol in 1 h of reaction time.

Catalyst	Catalyst [mg]	TOF [h <sup>-1</sup> ] <sup>[a]</sup>	Conv. [%]	Selectivity [%] <sup>[b]</sup>		
				2-Brth	4-Brth	2,4-diBrth
[W <sup>VI</sup> O <sub>2</sub> L <sup>1</sup> ] (1)	1.0	6596	93	14	76	10
[W <sup>VI</sup> O <sub>2</sub> L <sup>2</sup> ] (2)	1.0	5975	95	12	63	25
[W <sup>VI</sup> O <sub>2</sub> L <sup>3</sup> ] (3)	1.0	4891	90	13	63	24
[W <sup>VI</sup> O <sub>2</sub> L <sup>4</sup> ] (4)	1.0	5313	85	12	60	28
Without catalyst		–	18	08	70	22

[a] TOF values calculated at 1 h reaction time. [b] 2-Brth = 2-bromothymol, 4-Brth = 4-bromothymol and 2,4-diBrth = 2,4-dibromothymol.

different amounts of KBr (10, 15 and 20 mmol) were taken in 20 mL water. Three different amounts of 70 % aqueous HClO<sub>4</sub> (10, 15 and 20 mmol) was added in two equal portions as pointed out in the experimental section to avoid the decomposition of complex and the reaction was carried out at room temperature for 2 h.

Details of all reaction conditions and the corresponding conversions of thymol are summarized in Table 7. Figure S5 provide time on conversion of thymol under different reaction conditions. It may be concluded from the data presented in table that conversion of thymol differs considerably under different reaction conditions. In general, though 4-bromothymol is obtained in highest yield under all conditions along with other two products, conditions under entry 8 is suitable to achieve mainly two monobromo products in major yields along with 80 % conversion. However, entry 2 presents the best suited conditions (i.e. for 10 mmol of substrate, the catalyst:substrate:H<sub>2</sub>O<sub>2</sub>:KBr:HClO<sub>4</sub> ratios are 1.59 ×

10<sup>-3</sup>:1:2:2:2) for the maximum conversion of thymol. Under these conditions, reaction reaches to equilibrium in 1 h and the obtained conversion is 95 % where the selectivity of three bromo products follows the order: 4-bromothymol (63 %) > 2,4-dibromothymol (25 %) > 2-bromothymol (12 %).

Other three catalysts i.e. 1, 3 and 4 were also tested considering 1.0 mg of each under the above optimized reaction conditions and the results are accessible in Table 8. It is clear from the data of table that other three complexes are also active and give 85–93 % conversion (also see Figure 9) with high turnover frequency. Again 4-bromothymol is highest in selectivity in all cases. Blank reaction i.e. without catalyst under these conditions gave only 18 % and 32 % conversion of thymol in 1 h and 2 h, respectively. We have also checked the activity of Na<sub>2</sub>WO<sub>4</sub> and WO<sub>3</sub>·H<sub>2</sub>O (using same mole equivalent as for 1) under above optimized reaction conditions (Table 7) and obtained conversions 70 and 68 %, respectively, are in line of

**Table 7.** Conversion of thymol (1.50 g, 10 mmol) using 2 as a catalyst, turn over frequency (TOF), and selectivity of different products at different reaction time under different reaction conditions.

Entry	KBr [g (mmol)]	H <sub>2</sub> O <sub>2</sub> [g (mmol)]	HClO <sub>4</sub> [g (mmol)]	Catalyst [mg (mmol)]	Conv. [%]	Time [h]	TOF <sup>[a]</sup> [h <sup>-1</sup> ]	Selectivity [%] <sup>[b]</sup>		
								a	b	c
1	2.38 (20)	2.26 (20)	2.86 (20)	0.5 (7.98 × 10 <sup>-4</sup> )	88	1	11027	11	55	34
2 <sup>[c]</sup>	2.38 (20)	2.26 (20)	2.86 (20)	1.0 (1.59 × 10 <sup>-3</sup> )	95	1	5975	12	63	25
3	2.38 (20)	2.26 (20)	2.86 (20)	1.5 (2.39 × 10 <sup>-3</sup> )	93	1	3891	12	67	21
4	2.38 (20)	2.26 (20)	2.86 (20)	2.0 (3.19 × 10 <sup>-3</sup> )	91	1	2853	12	56	32
5	2.38 (20)	1.69 (15)	2.86 (20)	1.0 (1.59 × 10 <sup>-3</sup> )	97	2	3053	13	77	10
6	2.38 (20)	1.13 (10)	2.86 (20)	1.0 (1.59 × 10 <sup>-3</sup> )	75	2	2358	14	83	03
7	1.78 (15)	2.26 (20)	2.86 (20)	1.0 (1.59 × 10 <sup>-3</sup> )	98	2	3082	13	75	12
8	1.19 (10)	2.26 (20)	2.86 (20)	1.0 (1.59 × 10 <sup>-3</sup> )	80	2	2516	14	84	02
9	2.38 (20)	2.26 (20)	2.15 (15)	1.0 (1.59 × 10 <sup>-3</sup> )	98	2	3082	14	77	09
10	2.38 (20)	2.26 (20)	1.43 (10)	1.0 (1.59 × 10 <sup>-3</sup> )	71	2	2233	14	76	10
11	2.38 (20)	2.26 (20)	2.86 (20)	blank	18	1	–	08	70	22

[a] TOF: Moles of substrate converted per mole of catalyst per hour. [b] a = 2-bromothymol, b = 4-bromothymol and c = 2,4-dibromothymol. [c] The optimized conditions mentioned in entry 2 are the best among the different sets of reactions carried out.

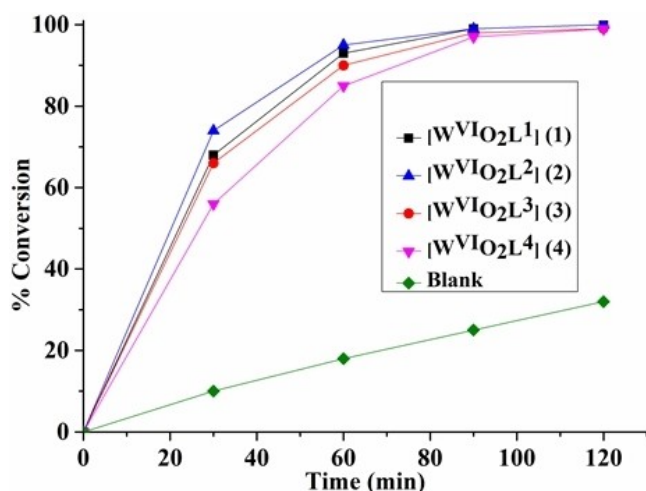


**Figure 9.** Plots representing conversion of thymol in the presence of different complexes as catalysts under aqueous phase. For reaction condition see Table 7.

the approval of no decomposition of complexes and their role in enhancing the conversion.

Different biphasic solvent systems have also been applied to understand the catalytic potential of complex 2 towards the oxidative bromination of thymol and their effect on the selectivity of different products. The catalytic efficiency of 2 under the optimised reaction conditions (see Table 7) except solvent:water (1:1 V/V, 20 mL) was found almost same in most mixed solvent systems studied (Table S3). The conversions are also comparable to the conversion obtained in aqueous system but the selectivity of products differs. In biphasic system, selectivity of 4-bromothymol is highest (57–69%) followed by 2,4-dibromophenol (19–33%) and then 2-bromophenol (5–14%). Thus, bi-phasic solvent systems alter the selectivity of products.

The catalytic potential of the complexes studied here are equally good or slightly better than [V<sup>VO</sup>]<sub>2</sub>,<sup>[30–34]</sup> and [Mo<sup>VO</sup>]<sub>2</sub>,<sup>[35,36]</sup> and comparable to [W<sup>VO</sup>]<sub>2</sub> complexes of tridentate ONO donor Schiff base ligands derived from 2-hydroxyacetophenone and nicotinoylhydrazide and benzoylhydrazide,<sup>[11]</sup> but selectivity of products slightly differs. The higher amounts of KBr, H<sub>2</sub>O<sub>2</sub> and HClO<sub>4</sub> (2 equivalents each for 10 mmol of substrate) versus lower amounts of these reagents for vanadium and molybdenum complexes might be responsible for such differences.

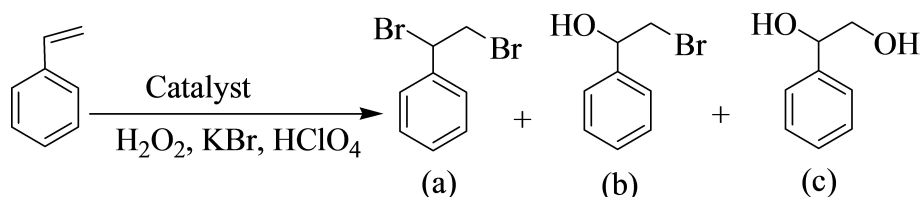
## Oxidative Bromination of Styrene

All these complexes have also been used as a catalyst to study the oxidative bromination of styrene. We have again considered complex 2 as a representative catalyst and the oxidative bromination of styrene was carried out at room temperature as detailed above and achieved the formation of 2-bromo-1-phenylethanol and 1-phenylethane-1,2-diol, though literature reports the formation of one more product i.e. 1,2-dibromo-1-phenylethane (Scheme 4).<sup>[30,31]</sup>

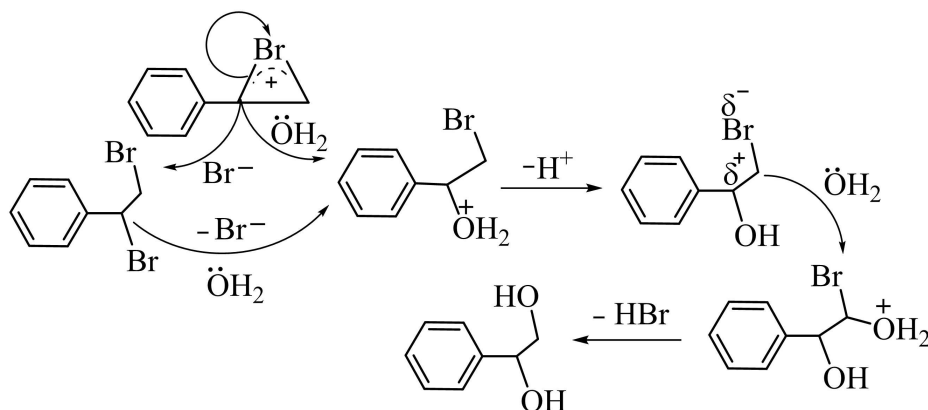
As observed in model *cis*-[MO<sub>2</sub>] complexes (M=V or Mo),<sup>[26–31,35]</sup> the generated HOBr and/or Br<sup>+</sup>, Br<sub>2</sub>, Br<sup>3+</sup>, through catalytic reaction of these complexes with H<sub>2</sub>O<sub>2</sub> and HClO<sub>4</sub> in the presence of KBr, react with styrene to generate bromonium ion as an intermediate (Scheme 5). The nucleophile Br<sup>−</sup> as well as H<sub>2</sub>O both may further attack on the α-carbon of the intermediate to give 1,2-dibromo-1-phenylethane and 2-bromo-1-phenylethane-1-ol, respectively. Since 1,2-dibromo-1-phenylethane is not observed in the reaction studied here, it seems that the nucleophile H<sub>2</sub>O activates α- as well as β-carbons both of it to give 2-bromo-1-phenylethane-1-ol and 1-phenylethane-1,2-diol.<sup>[35,36]</sup> 2-Bromo-1-phenylethane-1-ol can further be converted to 1-phenylethane-1,2-diol through α-carbon hydrolysis and all these justify the formation of 1-phenylethane-1,2-diol in highest yield. Since, styrene may also give styrene epoxide in the presence of catalyst and oxidant, which can then undergo nucleophilic attack, either from bromide or water to give the observed products, such possibility has, however, been excluded as we did not observe the formation of styrene epoxide.

Subsequently, the catalytic reaction was investigated by changing different parameters as mentioned above that may affect the rate of styrene bromination and the selectivity of different products. Details of all reaction conditions and the corresponding conversion of styrene are presented in Figure 10 (and data are summarized in Table S4). From the data presented in Table S4 it is clear that the optimized reaction conditions for the maximum conversion of 10 mmol (1.04 g) of styrene are those using 0.5 mg of catalyst, 1.69 g (15 mmol) of 30% aqueous H<sub>2</sub>O<sub>2</sub>, 2.38 g (20 mmol) of KBr, and 2.86 g (20 mmol) of 70% aqueous HClO<sub>4</sub> i.e. (entry no. 5 of Table S4). Under these conditions conversion reaches 90% in 1 h and the selectivity of the two products follows the order: 1-phenylethane-1,2-diol (78%) > 2-bromo-1-phenylethanol (22%).

Other three catalysts i.e. 1, 3 and 4 were also tested under the above optimized reaction conditions considering 0.5 mg each of these catalysts and the results are presented in



**Scheme 4.** Expected products upon oxidative bromination of styrene: (a) 1,2-dibromo-1-phenylethane, (b) 2-bromo-1-phenylethane-1-ol, and (c) 1-phenylethane-1,2-diol.



**Scheme 5.** Plausible mechanism of action of Br<sub>2</sub>/HOBr on styrene and hydrolysis of the brominated products in the presence of water.

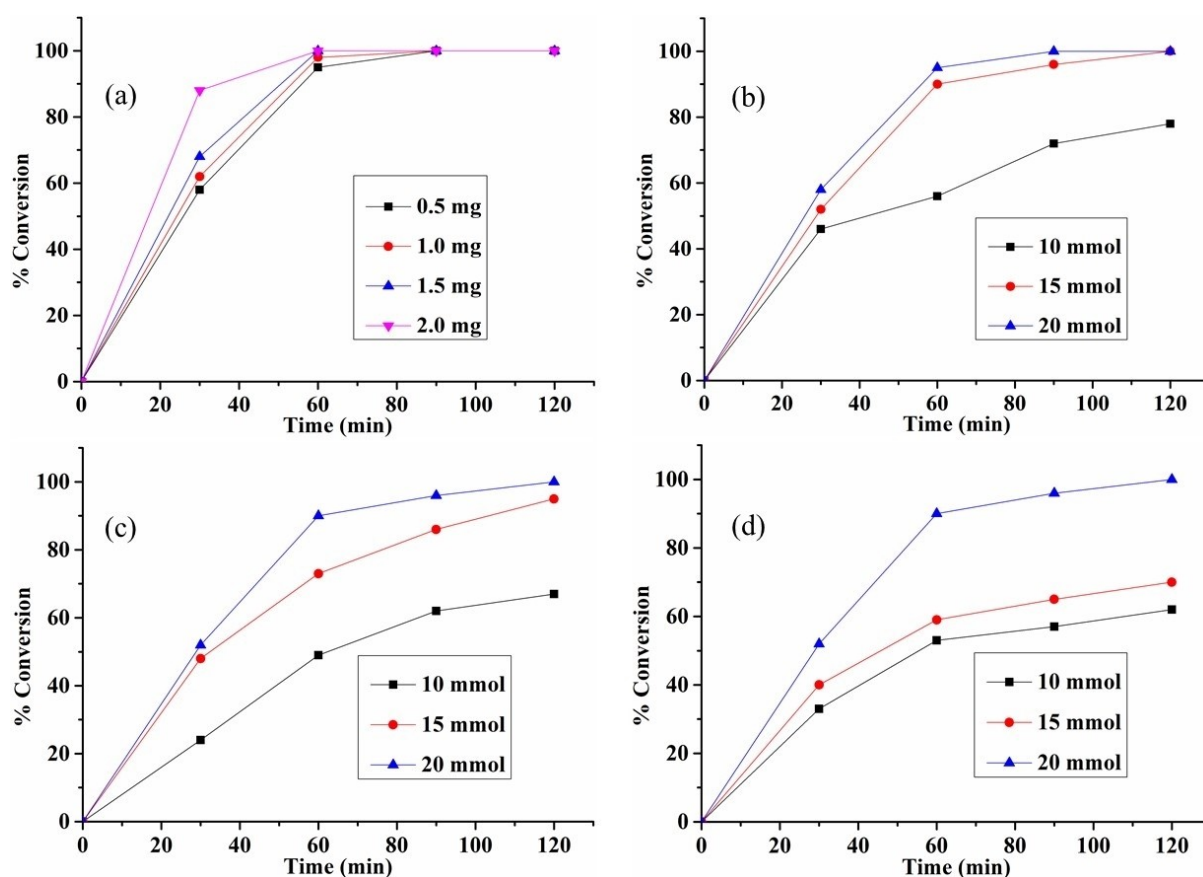


**Figure 10.** (a) Effect of variation of amount of catalyst on the oxidative bromination of styrene. Reaction conditions: styrene (1.04 g, 10 mmol), 30% aqueous H<sub>2</sub>O<sub>2</sub> (2.26 g, 20 mmol), KBr (2.38 g, 20 mmol), and HClO<sub>4</sub> (2.86 g, 20 mmol) at room temperature. (b) Effect of variation of amount of oxidant (H<sub>2</sub>O<sub>2</sub>) on the oxidative bromination of styrene. Reaction conditions: styrene (1.04 g, 10 mmol), catalyst [W<sup>VI</sup>O<sub>2</sub>L<sub>2</sub>] (0.5 mg, 7.98 × 10<sup>-4</sup> mmol), KBr (2.38 g, 20 mmol), and HClO<sub>4</sub> (2.86 g, 20 mmol) at room temperature. (c) Effect of variation of amount of KBr on the oxidative bromination of styrene. Reaction conditions: styrene (1.04 g, 10 mmol), catalyst [W<sup>VI</sup>O<sub>2</sub>L<sub>2</sub>] (0.5 mg, 7.98 × 10<sup>-4</sup> mmol), 30% aqueous H<sub>2</sub>O<sub>2</sub> (1.69 g, 15 mmol), and HClO<sub>4</sub> (2.86 g, 20 mmol) at room temperature. (d) Effect of variation of amount of HClO<sub>4</sub> on the oxidative bromination of styrene. Reaction conditions: styrene (1.04 g, 10 mmol), catalyst [W<sup>VI</sup>O<sub>2</sub>L<sub>2</sub>] (0.5 mg, 7.98 × 10<sup>-4</sup> mmol), 30% aqueous H<sub>2</sub>O<sub>2</sub> (1.69 g, 15 mmol), and KBr (2.38 g, 20 mmol) at room temperature.

Figure 11. It is clear from the figure that substituents on the ligands have not much influence and these complexes also have similar catalytic potential. Conversion between 88–93% with high TOF has been obtained in 1 h reaction time (Table 9).

Again 1-phenylethane-1,2-diol is highest in selectivity. Blank reaction under above reaction conditions gave only 19% and 33% conversion in 1 and 2 h, respectively.

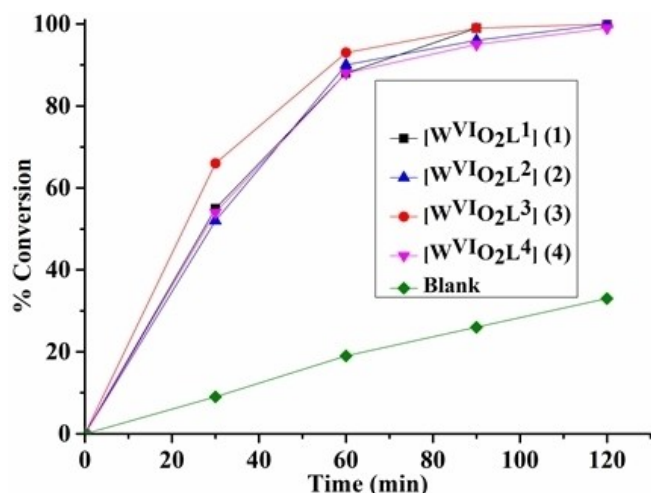


Figure 11. Plots presenting conversion of styrene in the presence of different complexes as catalyst.

Catalytic potential of **2** towards the oxidative bromination of styrene under different biphasic solvent systems (1:1 V/V, 20 mL) is almost same as observed in aqueous system. However, the selectivity of the formation of 1-phenylethane-1,2-diol (Table S5) is at slightly higher side (ca. 10%) than observed in aqueous solution.

## Conclusions

Four *cis*-dioxidotungsten(VI) complexes, *cis*-[W<sup>VI</sup>O<sub>2</sub>L<sup>1-4</sup>] (**1–4**) have been prepared from potential dibasic tetradentate ONNO salan-type Mannich base ligands derived from ethylenediamine and 2,4-di-*tert*-butylphenol(H<sub>2</sub>L<sup>1</sup>) (**I**), 2-*tert*-butyl-4-methylphenol (H<sub>2</sub>L<sup>2</sup>) (**II**), 2,4-di-methylphenol (H<sub>2</sub>L<sup>3</sup>) (**III**), and 2,4-di-chlorophenol (H<sub>2</sub>L<sup>4</sup>) (**IV**). All these complexes adopt  $\alpha$ -*cis*, symmetrical type configuration, a common isomeric form found in most complexes having *cis*-[MO<sub>2</sub>] (M=V, Mo and W) of salan-type ligands. DFT study predicts the poor stability of other two possible isomers. Oxidative bromination of thymol and styrene has been successfully carried out using these complexes as catalyst precursor, signifying them as useful functional model of vanadium dependent haloperoxidases. Phenol being *ortho*- and *para*-directing, the bromination on thymol gives three products, namely, 2-bromothymol, 4-bromothymol, and 2,4-dibromothymol

and as expected 2,4-dibromothymol is obtained in major yield. 2-Bromo-1-phenylethanol and 1-phenylethane-1,2-diol were obtained upon oxidative bromination of styrene, though 1,2-dibromo-1-phenylethane was also an expected product. The H<sub>2</sub>O, a nucleophile, present in the oxidant H<sub>2</sub>O<sub>2</sub> possibly activates  $\alpha$ - as well as  $\beta$ -carbons both of 1,2-dibromo-1-phenylethane which allows it to undergo further hydrolysis to give other products.

## Experimental Section

### Materials and General Methods

WO<sub>2</sub>Cl<sub>2</sub>, acetylacetone (SRL, India), 2,4-di-*tert*-butylphenol, 2,4-dimethylphenol, 2-*tert*-butyl-4-methylphenol, 2,4-dichlorophenol, ethylenediamine, formaldehyde and toluene (Rankem, India) were used as supplied. Toluene was dried over sodium and distilled before use. Other chemicals and solvents were of AR grade. Ligands H<sub>2</sub>L<sup>1-4</sup> were prepared following literature method.<sup>[18]</sup>

All measurements were carried out after drying the metal complexes at 100 °C. Elemental analyses of the complexes were carried out on an Elementar model Vario-EI-III. Thermogravimetric analyses of the complexes were carried out using a Perkin Elmer (Pyris Diamond) instrument in air with a heating rate of 10 °C/min between room temperature to 1000 °C. IR spectra were recorded as KBr pellets on a Nicolet 1100 FT-IR spectrometer. UV-visible spectra of ligands and complexes were recorded in acetonitrile on a Shimadzu 2600 UV-vis spectrophotometer. <sup>1</sup>H and <sup>13</sup>C NMR spectra were recorded in d<sub>6</sub>-[DMSO] on a JEOL ECX 400 MHz spectrometer. All the electrochemical measurements were carried out using instrument (HCH-620 E) under the argon atmosphere assembled with typical three-electrode assembly. The cyclic voltammogram (CV) and differential pulse voltammetric (DPV) of redox active ligands (**I–IV**) and *cis*-[W<sup>VI</sup>O<sub>2</sub>] complexes (**1–4**) were recorded in the range of –2.0 V to +2.0 V vs. SCE using Pt working electrode, Ag/AgCl reference electrode and Pt wire as counter electrode. Tetrabutyl ammonium hexafluorophosphate (TBAPF<sub>6</sub>), crystallized twice from EtOH and vacuum dried, was used as supporting electrolyte in distilled dichloromethane with a 100 mV/s scan rate at room temperature (ca. 298 K). The concentration of these newly synthesized complexes was maintained ca. 1 mM during the electrochemical analysis. A Shimadzu 2010 plus gas-chromatograph fitted with a Rtx-1 capillary column (30 m × 0.25 mm × 0.25  $\mu$ m) and a FID detector was used to analyze the reaction products and their quantifications were made on the basis of the relative peak area of the respective product. The identity of the products was confirmed using a GC-MS model PerkinElmer, Clarus 500 and comparing the fragments of each product with the library available.

Table 9. Conversion, turn over frequency and selectivity parameters for various catalysts for the oxidative bromination of styrene in 1 h of reaction time.

Catalyst	Catalyst [mg]	TOF [h <sup>-1</sup> ]	Conv. [%]	Selectivity [%] <sup>[a]</sup> b	c
[W <sup>VI</sup> O <sub>2</sub> L <sup>1</sup> ] ( <b>1</b> )	0.5	12518	88	32	68
[W <sup>VI</sup> O <sub>2</sub> L <sup>2</sup> ] ( <b>2</b> )	0.5	11278	90	22	78
[W <sup>VI</sup> O <sub>2</sub> L <sup>3</sup> ] ( <b>3</b> )	0.5	10087	93	39	61
[W <sup>VI</sup> O <sub>2</sub> L <sup>4</sup> ] ( <b>4</b> )	0.5	10986	88	30	70
Without catalyst	–	–	19	18	82

[a] For details of 'b' and 'c' see Scheme 4.



## Preparations

Preparation of  $[W^VI O_2(acac)_2]$ 

This was prepared by a slightly modified method reported in the literature.<sup>[37,38]</sup> To a suspension of  $W^VI O_2 Cl_2$  (3.1 g, 10.78 mmol) in a freshly distilled 2,4-pentanedione (30 mL), dry toluene (100 mL) was added and the resulting mixture was refluxed for 36 h with constant stirring. Reflux condenser was fitted with a guard tube filled with  $CaCl_2$  during this period. The resulting mixture was filtered while still hot and solvent was removed completely from the filtrate using rotatory evaporator to yield a light-yellow crude product. The solid was collected after washing several times with diethyl ether. Yield: 3.30 g (74.0%). Solid is pure enough to use for the synthesis purpose.

Preparation of  $[W^VI O_2 L^1]$  (1)

A filtered solution of  $[W^VI O_2(acac)_2]$  (0.455 g, 1.1 mmol) in MeOH (20 mL) was added to a solution of  $H_2 L^1$  (0.496 g, 1.0 mmol) in MeOH (30 mL) and the obtained reaction mixture was refluxed with slow and constant stirring in an oil bath for 16 h. A light cream solid precipitated out upon reducing the solvent volume to ca. 10 mL and cooling the reaction mixture to room temperature, which was filtered, washed with cold methanol, and dried under vacuum. Yield 0.550 g (77.0%). Anal. Calcd for  $C_{32}H_{50}N_2O_4W$  (710.60 g mol<sup>-1</sup>): C, 54.1; H, 7.1; N, 3.9. Found: C, 54.5; H, 7.4; N, 4.5%. IR (KBr) : 3260 (NH), 940 (O=W=O)<sub>asym</sub>, 895 (O=W=O)<sub>sym</sub> cm<sup>-1</sup>. UV-vis (MeCN, ε/ litre mole<sup>-1</sup>cm<sup>-1</sup>): λ = 238 (2.27 × 10<sup>4</sup>), 279 (1.91 × 10<sup>4</sup>) nm.

Preparations of  $[W^VI O_2 L^2]$  (2),  $[W^VI O_2 L^3]$  (3) and  $[W^VI O_2 L^4]$  (4)

Complexes 2–4 were prepared following above method using  $[W^VI O_2(acac)_2]$  (0.455 g, 1.1 mmol) and respective ligands (1.0 mmol). All complexes have almost same cream coloured solid.

$[W^VI O_2 L^2]$  (2). Yield 0.440 g (70.0%). Anal. Calcd for  $C_{26}H_{38}N_2O_4W$  (626.44 g mol<sup>-1</sup>): C, 49.9; H, 6.1; N, 4.5. Found: C, 50.3; H, 6.2; N, 4.9%. IR (KBr) : 3300 (NH), 922 (O=W=O)<sub>asym</sub>, 889 (O=W=O)<sub>sym</sub> cm<sup>-1</sup>. UV-vis (MeCN, ε/ litre mole<sup>-1</sup>cm<sup>-1</sup>): λ = 237 (3.05 × 10<sup>4</sup>), 282 (2.61 × 10<sup>4</sup>) nm.

$[W^VI O_2 L^3]$  (3). Yield 0.477 g (88.0%). Anal. Calcd for  $C_{20}H_{26}N_2O_4W$  (542.28 g mol<sup>-1</sup>): C, 44.3; H, 4.8; N 5.2. Found: C, 45.0; H, 4.7; N 5.3%. IR (KBr) : 3182, 3295 (NH), 942 (O=W=O)<sub>asym</sub>, 886 (O=W=O)<sub>sym</sub> cm<sup>-1</sup>. UV-vis (MeCN, ε/ litre mole<sup>-1</sup>cm<sup>-1</sup>): λ = 238 (2.96 × 10<sup>4</sup>), 281 (2.71 × 10<sup>4</sup>) nm.

$[W^VI O_2 L^4]$  (4). Yield 0.523 g (84.0%). Anal. Calcd for  $C_{16}H_{14}Cl_4N_2O_4W$  (623.94 g mol<sup>-1</sup>): C, 30.8; H, 2.3; N 4.5. Found: C, 30.5; H, 2.4; N, 4.7%. IR (KBr) : 3220 (NH), 940 (O=W=O)<sub>asym</sub>, 901 (O=W=O)<sub>sym</sub> cm<sup>-1</sup>. UV-vis (MeCN, ε/ litre mole<sup>-1</sup>cm<sup>-1</sup>): λ = 242 (2.33 × 10<sup>4</sup>), 278 (1.99 × 10<sup>4</sup>) nm.

## X-ray Crystal Structure Determination

Three-dimensional X-ray data were collected on a Bruker Kappa Apex CCD diffractometer at room temperature for 2 and 3 by the  $\phi$ - $\omega$  scan method. Reflections were measured from a hemisphere of data collected from frames, each of them covering 0.3° in  $\omega$ . A total of 63818 for 2 and 32962 for 3 reflections measured were corrected for Lorentz and polarization effects and for absorption by multi-scan methods based on symmetry-equivalent and repeated reflections. A total of 6361 for 2 and 4338 for 3, independent reflections exceeded the significance level ( $|F|/\sigma|F|$ ) > 4.0, respectively. After data collection, in each case an empirical absorption

correction (SADABS)<sup>[39]</sup> was applied, and the structures were solved by direct methods and refined by full matrix least-squares on  $F^2$  data using SHELX suite of programs.<sup>[40,41]</sup> All hydrogen atoms were placed in geometrically calculated positions using a riding model except for N1 and N2 which were located in difference Fourier map and left to refine freely. Refinements were done with allowance for thermal anisotropy of all non-hydrogen atoms. A final difference Fourier map showed no residual density outside: 1.1432 and -1.3566 for 2 and 2.3074 and -2.0994 for 3. A weighting scheme  $w = 1/[\sigma^2(F_o^2) + (0.021322 P)^2 + 6.383177P]$  for 2 and  $w = 1/[\sigma^2(F_o^2) + (0.060902 P)^2 + 0.00000 P]$  for 3, where  $P = (|F_o|^2 + 2|F_c|^2)/3$ , were used in the latter stages of refinement. Further details of the crystal structure determination are given in Table 10.

## Catalytic Activity Studies

All catalytic reactions were carried out in a 50 mL round bottom flask and a similar procedure was adopted for all complexes used as catalyst. A typical reaction for each substrate is provided below:

**Oxidative Bromination of Thymol** Thymol (1.5 g, 10 mmol), 30% aqueous  $H_2O_2$  (1.13 g, 10 mmol), KBr (1.19 g, 10 mmol), 70% aqueous  $HClO_4$  (1.43 g, 10 mmol) were taken in 20 mL water. After adding a representative tungsten complex 2 as catalyst (1.0 mg), the reaction mixture was stirred for 2 h at room temperature. The best reaction condition for the bromination of thymol was identified by varying several parameters, such as the amount of catalyst, KBr,  $H_2O_2$  and  $HClO_4$ . When addition of  $HClO_4$  was more than 10 mmol, it was added in two portions: first 10 mmol addition at  $t=0$  and the other at  $t=0.5$  h to avoid decomposition of the catalyst. The progress of the reaction was monitored by withdrawing small aliquot of the reaction mixture, extracting it from hexane and analysing by GC. The quantification of the brominated products was made on the basis of the relative peak area of the respective product and their identities were established by GC-MS and <sup>1</sup>H NMR spectroscopy.

Table 10. Crystal data and structure refinement for  $[W^VI O_2 L^2]$  (2) and  $[W^VI O_2 L^3]$  (3).

	2	3
Formula	$C_{26}H_{38}W N_2 O_4$	$C_{20}H_{26}W N_2 O_4$
Formula weight	626.44	542.28
T, K	296.15	296.15
Wavelength, Å	0.71073	0.71073
Crystal system	Orthorhombic	Monoclinic
Space group	Pbca	P2 <sub>1</sub> /n
a/Å	13.9899(10)	12.2661(19)
b/Å	12.887(1)	11.0763(17)
c/Å	28.321(2)	15.761(2)
α/°	90	90
β/°	90	111.740(2)
γ/°	90	90
V/Å <sup>3</sup>	5105.9(7)	1989.0(5)
Z	8	4
F <sub>000</sub>	2509.7	1062.8
D <sub>calc</sub> /g cm <sup>-3</sup>	1.630	1.811
μ/mm <sup>-1</sup>	4.558	5.835
θ/°	2.88 to 28.37	3.26 to 27.46
R <sub>int</sub>	0.0321	0.1711
Crystal size/ mm <sup>3</sup>	0.31 × 0.21 × 0.16	0.48 × 0.41 × 0.35
Goodness-of-fit on F <sup>2</sup>	1.089	0.974
R <sub>1</sub> [I > 2σ(I)] <sup>[a]</sup>	0.0219	0.0393
wR <sub>2</sub> (all data) <sup>[b]</sup>	0.0571	0.1029
Largest differences peak and hole (eÅ <sup>-3</sup> )	1.14 and -1.36	2.31 and -2.10
[a] $R_1 = \sum   F_o  -  F_c   / \sum  F_o $ . [b] $wR_2 = \{\sum [w( F_o ^2 -  F_c ^2)]^2 / \sum [w(F_o^2)^2]\}^{1/2}$ .		



## FULL PAPERS



Prof. Dr. M. R. Maurya\*, S. K. Maurya,  
N. Kumar, Dr. P. Gupta

1 – 16

**Biomimetic Oxidative Bromination  
by *cis*-Dioxidotungsten(VI)  
Complexes of *salan* type N,N'-  
Capped Linear Tetradentate  
Amino Bisphenol**



Six-coordinated octahedral  $\alpha$ -*cis*,  
symmetric isomeric form of the *cis*-  
[WO<sub>2</sub>L] complexes of N,N'-capped  
linear tetradentate amino bisphenol

have been synthesized and used as  
catalyst for the oxidative bromination  
of thymol and styrene.